Journal of Inflammation Research Dovepress

Open Access Full Text Article ORIGINAL RESEARCH

Network Pharmacology and Machine Learning Reveal Salidroside's Mechanisms in Idiopathic Pulmonary Fibrosis Treatment

Chenchun Ding[1], Zhenzhen Guo[2], Quan Liao[1], Renjie Zuo[1], Junjie He[1], Ziwei Ye[2], Weibin Chen[1]

[1]Department of Thoracic Surgery, Zhongshan Hospital of Xiamen University, School of Medicine, Xiamen University, Xiamen, Fujian, 361102, People's Republic of China; [2]School of Pharmaceutical Sciences, Xiamen University, Xiamen, Fujian, 361102, People's Republic of China

Correspondence: Weibin Chen, Department of Thoracic Surgery, Zhongshan Hospital of Xiamen University, School of Medicine, Xiamen University, Xiamen, Fujian, 361102, People's Republic of China, Email cwbxmu@163.com

Purpose: Idiopathic pulmonary fibrosis (IPF) is an irreversible respiratory disease. In this study, we evaluated the efficacy of salidroside (SAL), the main component of Rhodiola rosea, in treating IPF.

Methods: The pharmacological effects of SAL against epithelial-mesenchymal transition (EMT) and IPF were assessed through in vivo and in vitro experiments. Targets for SAL in treating IPF were identified from various databases and a PPI network was constructed. Functional analyses of target genes were performed using GO, KEGG, DO, and GSEA. Core target genes were identified using LASSO logistic regression and support vector machine (SVM) analysis, followed by molecular docking simulations. Predicted targets and pathways were validated through Western blotting, qRT-PCR, and IHC.

Results: Our results demonstrated that SAL ameliorated alveolar epithelial cells (AECs) EMT and mitigated bleomycin -induced pulmonary fibrosis. Through network pharmacology, we identified 74 targets for SAL in the treatment of IPF (P_{FDR}<0.05) and analyzed their biological functions. Based on these findings, we further applied machine learning techniques to narrow down 9 core targets (P_{FDR}<0.05). Integrating the results from molecular docking, KEGG, and GSEA analyses, we selected three key targets—IGF1, hypoxia-inducible factor 1-alpha (HIF-1α), and MAPK (P_{FDR}<0.05)—for further investigation. Our study revealed that SAL inhibits the IGF1 signaling pathway, thereby improving AECs senescence and cell cycle arrest. By inhibiting the HIF-1α pathway, SAL alleviates endoplasmic reticulum stress and reduces intracellular ROS accumulation. Moreover, SAL suppresses the activation of the MAPK signaling pathway, leading to a decrease in inflammation markers in AECs and lung tissue.

Conclusion: Experimental results suggest that SAL effectively ameliorates BLM-induced EMT and IPF, likely through the inhibition of IGF1, HIF-1α, and MAPK signaling pathways. This study holds potential translational prospects and may provide new perspectives and insights for the use of traditional Chinese medicine in the treatment of IPF.

Keywords: salidroside, idiopathic pulmonary fibrosis, network pharmacology, machine-learning, molecular docking

Introduction

Idiopathic pulmonary fibrosis (IPF) is a chronic and irreversible disease characterized by epithelial-mesenchymal transition (EMT) and excessive accumulation of extracellular matrix (ECM).[1,2] The global incidence of IPF is approximately 1–13 cases per 100,000 people, with a median survival time of only 3–8 years.[3,4] The etiology of IPF is complex, involving key mechanisms such as aging, chronic inflammation, oxidative stress, and genetic factors.[5] Currently, the main FDA-approved treatments—nintedanib and pirfenidone—focus on slowing disease progression.[6] Nintedanib, a tyrosine kinase inhibitor, blocks fibrosis-promoting pathways and reduces the decline in lung function (FVC).[7] However, it causes side effects like diarrhea and liver enzyme elevation, and does not reverse damage.[8] Pirfenidone has anti-inflammatory and anti-fibrotic properties, but its exact mechanism is unclear.[9] It slows FVC decline, though common side effects include nausea and liver toxicity.[10] Other therapies, like anti-fibrotic drugs, stem cell therapy, and lung transplantation, offer potential but face challenges such as safety concerns, limited efficacy, and donor shortages.[11–13] Current treatments only slow IPF progression,

Received: 16 September 2024
Accepted: 19 November 2024
Published: 22 November 2024

and research is ongoing to develop more effective therapies targeting fibrosis mechanisms. Given that traditional Chinese medicines (TCM) are often characterized by their multi-target and low-toxicity properties, exploring effective natural compounds from TCM for combating IPF may provide new avenues for treatment.

Rhodiola rosea, a traditional Chinese medicinal herb, predominantly grows in high-altitude, cold regions.[14] According to TCM, the rhizome, which is the medicinal part of the plant, is believed to have anti-fatigue, anti-aging, and altitude sickness prevention properties.[15–17] The main active compound in Rhodiola rosea, salidroside (SAL), is a phenylpropanoid glycoside monomer.[18] Recent studies have confirmed that SAL exhibits antioxidant, anti-inflammatory, and organ-protective effects. In liver protection, SAL has been shown to treat liver injury via the IRE1α/JNK signaling pathway by inhibiting endoplasmic reticulum stress-mediated apoptosis, thereby protecting against hypoxia-induced liver injury.[19] The potential of SAL in asthma treatment has also been demonstrated, as it can inhibit bronchial hyperreactivity and alleviate airway inflammation.[20] SAL suppresses the inflammatory response and the production of HMGB1 in macrophages and mice treated with bacterial lipopolysaccharide, effectively reducing sepsis-induced pulmonary edema, lipid peroxidation, histopathological changes, and mortality.[21] Moreover, it has been found to have renoprotective effects, as SAL treatment significantly reduces the release of inflammatory cytokines in kidney tissue, improves ECM component deposition, and lowers the levels of EMT markers in both mouse kidneys and HK-2 cells.[22] However, the potential of SAL in treating IPF remains unclear.

Previous studies have extensively reported on the pharmacological effects of SAL. However, these studies have several limitations, such as focusing primarily on phenotypic observations, lack of mechanistic insights, limited exploration of single pathways, and the absence of systematic, multi-pathway comparative studies. In this study, we adopt a holistic perspective on the association network between SAL and IPF disease targets, while applying machine learning to further enhance the reliability of target prediction. The predicted results are validated through molecular experiments, effectively mitigating the potential inaccuracies of computational predictions and elucidating the potential mechanisms of SAL in treating IPF from multiple dimensions. Network pharmacology is an approach that integrates systems biology and computational tools to study the interactions between drugs, targets, and biological networks, which aims to develop multi-target drugs that can affect multiple biological pathways simultaneously.[23] Machine learning and molecular docking techniques were employed to further screen the core target genes of SAL for IPF treatment, enhancing the accuracy of target prediction. Based on the results from integrated network pharmacology, machine learning, and molecular docking, three key pathways—Insulin-like Growth Factor 1 (IGF1), Hypoxia-Inducible Factor 1-alpha (HIF-1α), and Mitogen-Activated Protein Kinase (MAPK)—were ultimately identified. In vivo and in vitro experiments were conducted to validate the anti - IPF mechanisms of SAL.

Materials and Methods

Cell Culture

Alveolar epithelial cells (A549) were obtained from ATCC and maintained in DMEM high glucose medium (C7076-500mL, Bioss) supplemented with 10% fetal bovine serum and 1% streptomycin/penicillin. Cells were cultured at 37°C in a 5% CO2 atmosphere. Cells were seeded at a density of 3×10^4 cells and regularly passaged. Bleomycin (11-B608166, Boer) was dissolved in PBS, and SAL (mfcd00210553, Merck) was dissolved in PBS for cell treatment and stored at −20°C before use.

Pulmonary Fibrosis Animal Model

Six-week-old male C57BL/6 mice were purchased from the Xiamen University Laboratory Animal Center. Mice were anesthetized with 1% sodium pentobarbital (60 mg/kg), and bleomycin (BLM) (2 mg/kg in 40 μL sterile saline) was administered intratracheally. Control mice received the same volume of sterile saline. Starting on day 10 post-BLM injection, SAL (mfcd00210553, Merck) dissolved in saline (20, 40 mg/kg) was administered by gavage daily to anesthetized mice. Mice were sacrificed on day 20 post-BLM injection, and lung tissue samples were collected. On day 28 of SAL administration, mice were sacrificed after anesthesia. The mice were housed under specific pathogen-free (SPF) conditions with a 12-hour light/dark cycle and free access to food and water. All procedures involving animals were approved by the Institutional Animal Care and

Use Committee (IACUC) of Xiamen University (ethics approval number: XMULAC20240176). The animals used in this study were handled following the Guide for the Care and Use of Laboratory Animals published by the National Institutes of Health.

CCK - 8 Assay

A549 cells (3×10^4/mL) were seeded in 96 - well plates and treated with different concentration gradients of SAL (0 μM, 30 μM, 60 μM, 120 μM) for 24 hours and BLM (10 μM, 15 μM, 20 μM, 25 μM) for 72 hours according to the CCK-8 assay kit instructions. After treatment, the 96-well plates were incubated for 2 hours. OD values were measured using a microplate reader, with absorbance set at 450 nm. Cell viability was calculated as (OD value of test well - OD value of blank well) / (OD value of control well - OD value of blank well).

Histological Staining

Pulmonary tissues were collected from male C57BL/6 mice on day 28 after BLM or PBS treatment. The tissues were fixed in 4% paraformaldehyde, embedded in paraffin, and sectioned at 5 μm. Hematoxylin and eosin (H & E) (Solarbio), Masson's trichrome (Solarbio), and modified Sirius Red staining (Solarbio) were performed for histological evaluation.

Western Blot Analysis

Total protein was extracted using cold RIPA buffer with protease inhibitors. Protein concentration was measured using a BCA kit (BX-2142728, Pierce). Proteins were separated on 8–15% Tris-glycine SDS-PAGE gels at 80V, then 120V, and transferred to PVDF membranes (bsp0161, PALL). Membranes were blocked with 5% non-fat milk and probed with primary antibodies overnight at 4°C. After washing, membranes were incubated with secondary antibodies for 90 minutes at room temperature. Bands were visualized using a chemiluminescence imaging system (Biorad). Antibodies used in this study are listed in Supplementary Table 1.

Real-Time Fluorescence Quantitative PCR (qRT-PCR) Analysis

Total RNA was extracted from A549 cells and lung tissues using TRIzol reagent (YZ-15596018, Acmec). RNA concentration was measured with a NanoDrop One spectrophotometer (Thermo). cDNA was synthesized using Hifair® II Reverse Transcriptase (11110ES92*Yeasen) under the following conditions: 25°C for 5 minutes, 42°C for 40 minutes, and 85°C for 5 minutes. Amplification was performed using Hieff® qRT-PCR SYBR Green Master Mix (11203 ES08, Yeasen) with the following cycling conditions: 95°C for 5 minutes, followed by 40 cycles of 95°C for 10 seconds, 60°C for 20 seconds, and 72°C for 20 seconds. GAPDH was used as the internal control, and all data were normalized to the control. The mRNA sequences are listed in Supplementary Table 2.

Immunofluorescence Staining

Fresh pulmonary tissues were used to prepare frozen sections, which were fixed in acetone and blocked with goat serum for 20 minutes. An adequate amount of properly diluted primary antibodies was added, and the sections were placed in a humid chamber (1:100) at 4 °C for 12 hours. After removal from the refrigerator, they were allowed to equilibrate at room temperature for 45 minutes. Subsequently, the sec-tions were incubated with the appropriately diluted fluorescent secondary antibodies (1:400) for 1 hour. DAPI staining was performed, and the sections were sealed with a mounting medium containing an anti-fade reagent. Finally, images were captured using a high-sensitivity confocal laser scanning microscope (Zeiss LSM980). The primary antibodies used included Col1a1 (ab34710, Abcam), Fn (ab2413, Abcam), Sftpa1 (Shanghai Yaji), Sftpc (orb153398, Biorbyt). Secondary antibodies targeting different IgG species were Alexa Fluor® 594 (red) or 488 (green) conjugates (1:400, Invitrogen).

Target Acquisition for SAL

The molecular structure of SAL was obtained from the PubChem database (https://pubchem.ncbi.nlm.nih.gov/). Potential targets were identified using SwissADME (http://www.swissadme.ch/) and PharmMapper (http://www.lilab-ecust.cn/pharmmapper/). Target names were converted to gene names using UniProt (https://www.uniprot.org/).

Data Processing and DEG Analysis for IPF

Data were sourced from the GEO dataset (https://www.ncbi.nlm.nih.gov/geo/database). The study utilized the GSE21369 dataset (23 IPF samples and 6 normal samples),[24] the GSE10667 dataset (31 IPF samples and 15 normal samples),[25] and the GSE110147 dataset (22 IPF samples and 11 normal samples).[26] Data processing and DEG analysis were performed using R 4.4.1 software with the "limma" package for data normalization and differential expression analysis. Visualization of DEGs was conducted using the "ggplot2" package to produce volcano plots. In accordance with the regulations of the Medical Ethics Committee of Zhongshan Hospital, Xiamen University, the GEO dataset, being an existing open-access dataset, is exempt from ethical review.

Functional Enrichment of SAL Anti-IPF Target Genes

A Venn diagram (http://bioinformatics.psb.ugent.be/webtools/Venn/) was employed to identify the overlap between SAL target genes and IPF differentially expressed genes (DEGs), highlighting the potential therapeutic targets for SAL in treating IPF. To further investigate the mechanisms of these intersecting genes, the "clusterProfiler" R package was used to perform Disease Ontology (DO), Gene Ontology (GO), and Kyoto Encyclopedia of Genes and Genomes (KEGG) enrichment analyses. Gene function was assessed using GSEA version 4.1.0 software from the MSIGDB database via the Gene Set Enrichment Analysis (GSEA) website (http://software.broadinstitute.org/gsea/msigdb), utilizing a standard weighted enrichment method. One thousand permutations were applied for randomization. Hallmark, GO, and KEGG enrichment analyses were conducted for both high and low-risk groups using GSEA, with significant enrichment criteria set at FDR q-val < 0.25, |NES| > 1, and NOM p-val < 0.05.

Construction of the SAL and IPF Target Gene PPI Network

The intersecting targets of SAL and IPF were uploaded to the STRING database (https://string-db.org). Only human (Homo sapiens) was selected as the species, with a medium confidence level greater than 0.9. Data from the STRING database were then imported into Cytoscape 3.9.1 (NIGMS, USA) software to visualize the PPI network.

Machine Learning

The intersecting target genes of SAL and IPF were identified using machine learning algorithms: LASSO logistic regression and SVM-RFE. LASSO logistic regression was conducted using the "glmnet" package in R, and SVM-RFE was performed using the "e1071" package. The "Ggpubr" package was used to evaluate the expression levels of core genes via box plots. ROC curves were plotted using the "pROC" package in R, with GSE24206 as the external validation dataset, to assess the diagnostic accuracy of SAL treatment genes for IPF in the test dataset.

Molecular Docking

The crystal structures of protein targets were obtained from the PDB database (https://www.rcsb.org/). MGLTools software was utilized to remove small molecules and water molecules from the protein crystals while adding hydrogen atoms and charges. The two-dimensional structure of SAL was retrieved from the PubChem database and con-verted into a three-dimensional structure using ChemDraw. SAL was then applied as the ligand, with the protein target serving as the receptor. Molecular docking was performed using AutoDock Vina, and the results were analyzed using Discovery Studio.

Cell Cycle Analysis

After treatment with SAL and BLM, cells were digested with trypsin (containing EDTA) at 37°C, and digestion was terminated with DMEM containing FBS. The collected cells were washed twice with pre-chilled PBS, fixed in 70% ethanol at −20°C for 12 hours, and stained with propidium iodide (PI) using a Cell Cycle Detection Kit (C1052, Beyotime). Flow cytometry (Beckman CytoFlex) was used to analyze the cell cycle.

Senescence-Associated β-Galactosidase (SA-β-Gal) Staining

After treatment with SAL and BLM, SA-β-gal staining was performed using the SA-β-gal staining kit (G1580-100T, Solarbio) according to the manufacturer's instructions. The staining working solution was prepared according to the kit's instructions. The 6-well plate was sealed with plastic wrap to prevent evaporation, and cells were incubated at 37°C overnight. Senescent-positive cells were identified as blue-stained cells under an optical microscope.

ROS Analysis

A549 cells were seeded in a 24-well culture dish and treated with SAL and BLM. DCFH-DA (50101ES01, Yeasen) working solution was prepared by diluting DCFH-DA in serum-free culture medium at a 1:1000 dilution. Cells were incubated at 37°C for 30 minutes in the dark. After three washes with serum-free culture medium, the cells were observed directly under a fluorescence microscope after loading the probe.

Transmission Electron Microscopy (TEM)

Cells treated with SAL were harvested and immediately fixed in 2.5% glutaraldehyde overnight at 4 °C and post-fixed with 2% osmium tetroxide for 1 hour at 37 °C. Subsequently, cells were embedded and stained using uranyl acetate/lead citrate. The sections were imaged using a TEM (ThermoFisher Helios 5 UC).

Immunohistochemistry (IHC)

Mouse lung tissues were fixed in paraffin and sectioned into 5-μm-thick slices using a microtome. The sections were subjected to IHC staining. To detect p-p38 and p-ERK1/2, the sections were incubated overnight at 4°C with primary antibodies. The IHC staining was carried out using an immunohistochemical reagent (KIT-9720, MXB, China) following the manufacturer's protocol. Subsequent to staining with diaminobenzidine (DAB) solution (Servicebio, China), the slides were mounted and visualized under a light microscope (Nikon SMZ 1000). The primary antibodies employed included p-p38 (1:60, ab178867, Abcam) and p-ERK1/2 (1:60, ab201015, Abcam).

Statistical Analysis

R software 4.4.1 was employed in this study. DEGs screening, data processing, and DEG analysis between IPF and normal samples using a threshold of $P_{FDR} < 0.05$ and |log2 Fold Change (FC)| > 1. In the volcano plot, DEGs with log2FC < 0 were considered downregulated, while those with log2FC > 0 were considered upregulated.

The SPSS 20.0 software (SPSS Inc., Chicago, IL, USA) was used for statistical analysis. The data are represented by the mean ± SD. Statistical analyses were applied using the Student's *t*-test and one-way analysis of variance to determine statistical significance. Asterisks denote statistical significance (* $P < 0.05$, ** $P < 0.01$, *** $P < 0.001$, **** $P < 0.0001$, ns indicates no significance).

Results

In vivo Anti-EMT and in vitro Anti-Pulmonary Fibrosis Effects of SAL

First, using the CCK-8 assay, we determined the optimal concentrations of BLM and SAL. At a concentration of 25 μM, A549 cells exhibited reduced cell viability but a sufficiently high survival rate, making it more suitable for observation (Figure 1A). After exogenous supplementation with SAL, we observed a concentration-dependent increase in A549 cell viability, with the most significant effect at 120 μM (Figure 1B and C). In vivo experiments showed that SAL treatment significantly improved lung tissue remodeling, fibrosis, and inflammatory infiltration, as indicated by H&E staining results. Masson and Sirius Red staining demonstrated that SAL treatment reduced fibrous tissue and the accumulation of collagen I and collagen III in the lungs in a dose-dependent manner, with a more pronounced effect at 40 mg/kg compared to 20 mg/kg (Figure 1D). EMT is a crucial process in IPF pathogenesis, Western blot and qRT-PCR analysis revealed that SAL decreased the levels of EMT markers Col1a1 and Fn in A549 cells, while increasing the expression of epithelial markers Sftpa1 and Sftpc (Figure 1E–H). Immunofluorescence in mouse lung tissues also confirmed these

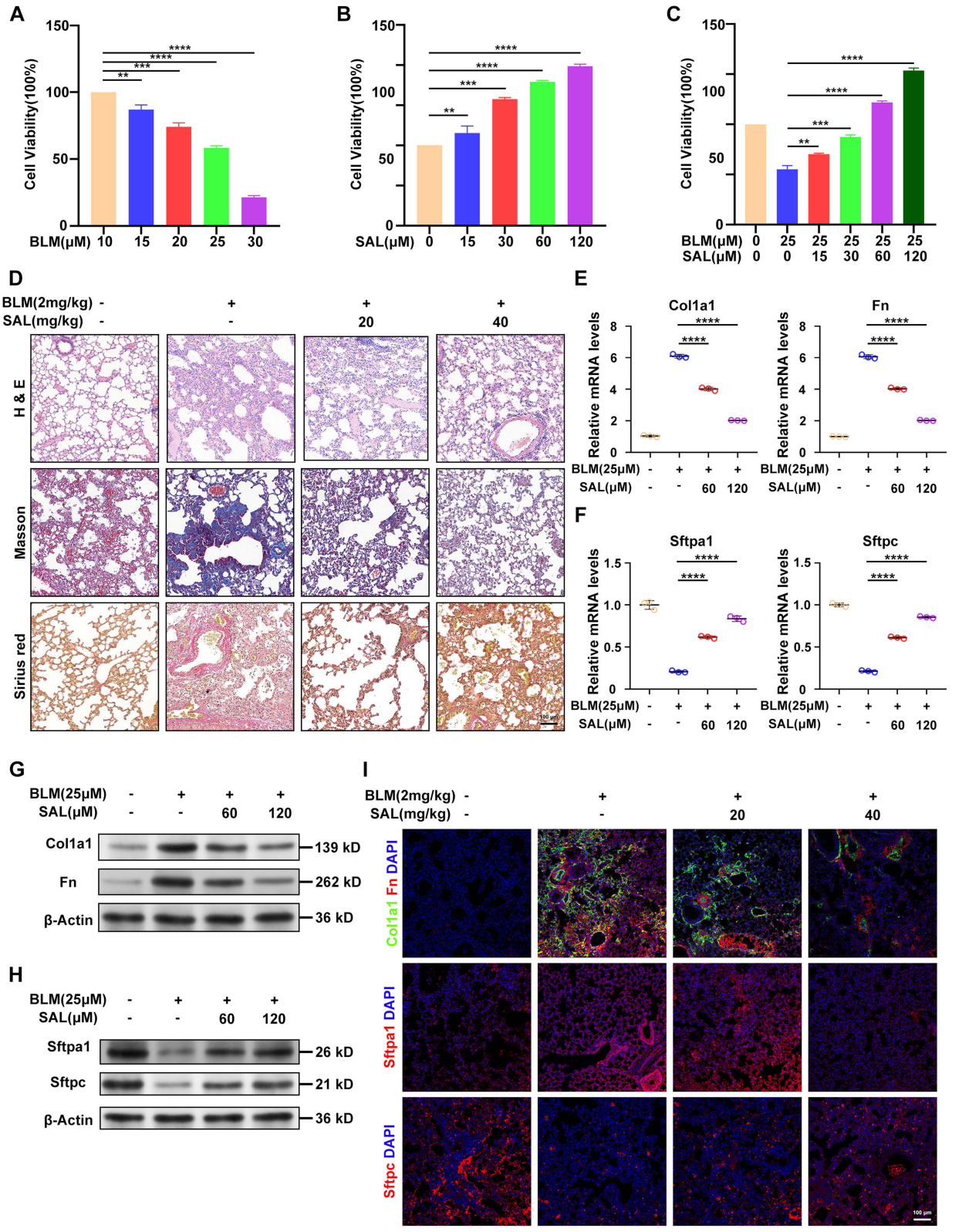

Figure 1 In Vivo Anti-EMT and In Vitro Anti-Pulmonary Fibrosis Effects of SAL: (**A**) A549 cells were treated with different concentrations of BLM for 72 hours. (**B**) A549 cells were treated with different concentrations of SAL for 24 hours. (**C**) A549 cells were initially treated with various concentrations of SAL for 24 hours, followed by treatment with25 μM BLM for 72 hours to induce senescence. (**D**) H & E, Masson's trichrome, and Sirius Red staining of lung tissue from mice treated with BLM and SAL. (**E** and **F**) The mRNA levels of Col1a1, Fn, Sftpa1, and Sftpc in A549 cells after BLM and SAL treatment were measured by qRT-PCR. (**G** and **H**) The protein expression levels of Col1a1, Fn, Sftpa1, and Sftpc in A549 cells after BLM and SAL treatment were deter-mined by Western blot analysis. (**I**) Immunofluorescence analysis of Col1a1, Fn, Sftpa1, and Sftpc expression levels in lung tissue from mice treated with BLM and SAL. Scale bars represent 100 μm in (**D** and **I**). In (**D–I**), - represents no drug treatment, and + represents drug treatment. Data in (**A–C, E and F**) are presented as mean ± SD (n = 3, **P < 0.01, ***P < 0.001, ****P < 0.0001; Student's *t*-test).

findings (Figure 1I). These results suggest that SAL effectively improves the EMT process caused by insufficient alveolar epithelial cell regeneration both in vivo and in vitro, thereby exerting anti-IPF effects.

Identification of SAL Targets in IPF Treatment

After removing duplicates, we obtained 358 target genes from the SwissADME and PharmMapper databases. From the GEO dataset, we identified 2455 DEGs as potential IPF targets, constructing a volcano plot (Figure 2A) that included 1293 upregulated genes and 1162 downregulated genes. The intersection of these two datasets yielded 74 target genes for SAL against IPF (Figure 2B). To further analyze the key targets of SAL, we constructed a PPI network of these 74 related targets, comprising 73 nodes and 228 edges (Figure 2C). Cytoscape 3.7.1 was used to create a SAL target network map (Figure 2D).

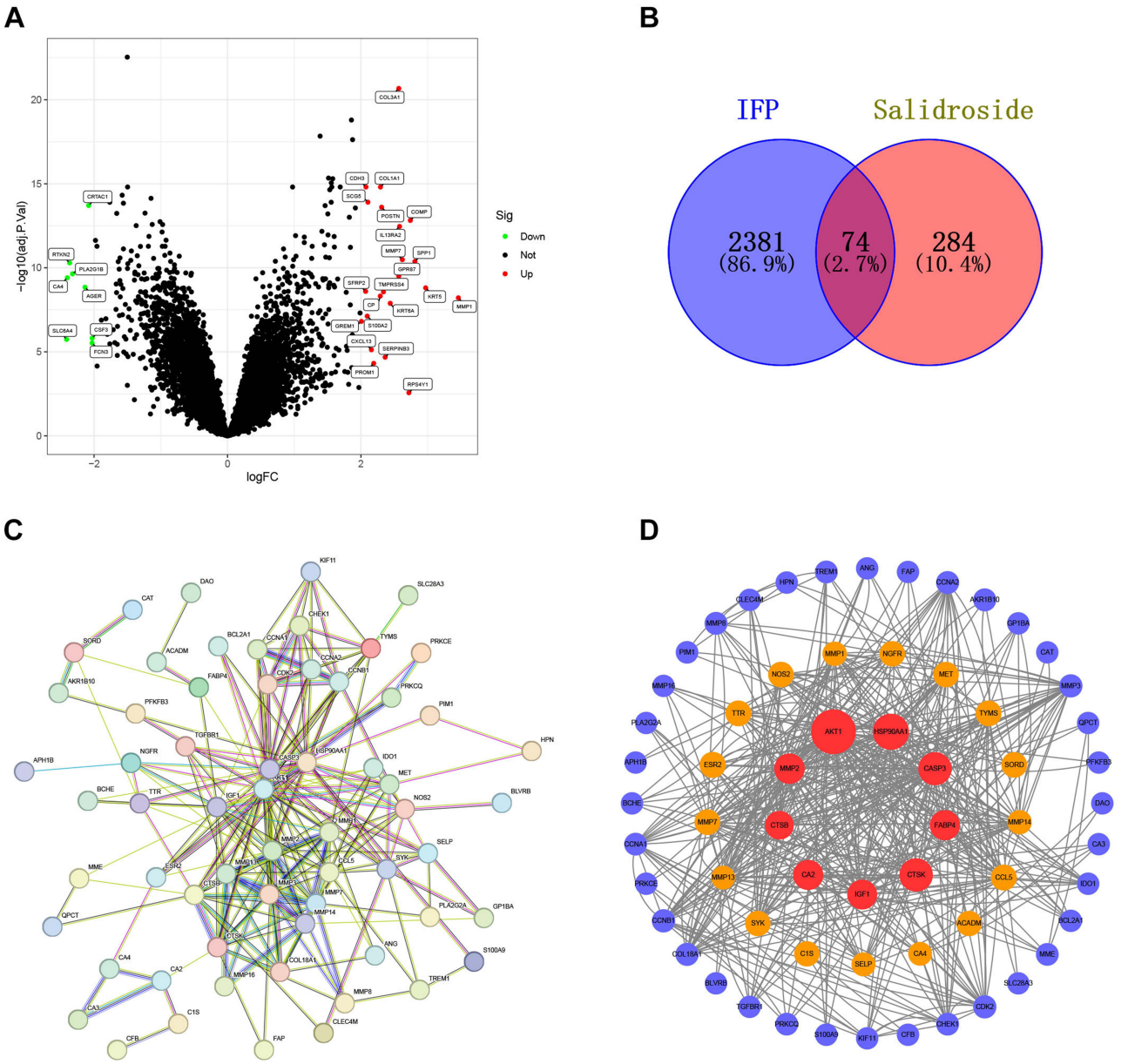

Figure 2 Identification of SAL Targets in IPF Treatment: (**A**) Volcano plot of the DEGs in IPF with the cut-off criteria of |log2FC|> 1 and false discovery rate (FDR) < 0.05. (**B**) Venn diagram showing the intersection of IPF DEGs and SAL target genes. (**C**) PPI network and hub gene identification. (**D**) Network diagram of SAL target genes. $P_{FDR} < 0.05$.

Functional Analysis of Common Targets of SAL in IPF Treatment

GO analysis indicated that the common targets of SAL in IPF treatment are involved in biological processes, including extracellular matrix organization, extracellular structure organization, external encapsulating structure organization, and leukocyte cell-cell adhesion. The cellular components (CC) related to DEGs include the apical part of the cell, secretory granule lumen, cytoplasmic vesicle lumen, and vesicle lumen cluster of actin-based cells. Molecular functions (MF) include endopeptidase activity, serine-type endopeptidase activity, serine-type peptidase activity, and serine hydrolase activity (Figure 3A). KEGG analysis showed that the treatment targets are mainly enriched in the AGE-RAGE signaling pathway in diabetic complications, progesterone-mediated oocyte maturation, MAPK signaling pathway, and HIF-1 signaling pathway (Figure 3B). DO analysis indicated that the treatment targets are significantly associated with interstitial lung disease (Figure 3C). GSEA results showed significant downregulation of the cytokine-cytokine receptor interaction, graft-versus-host disease, JAK-STAT signaling pathway, MAPK signaling pathway, and neuroactive ligand-receptor interaction pathways

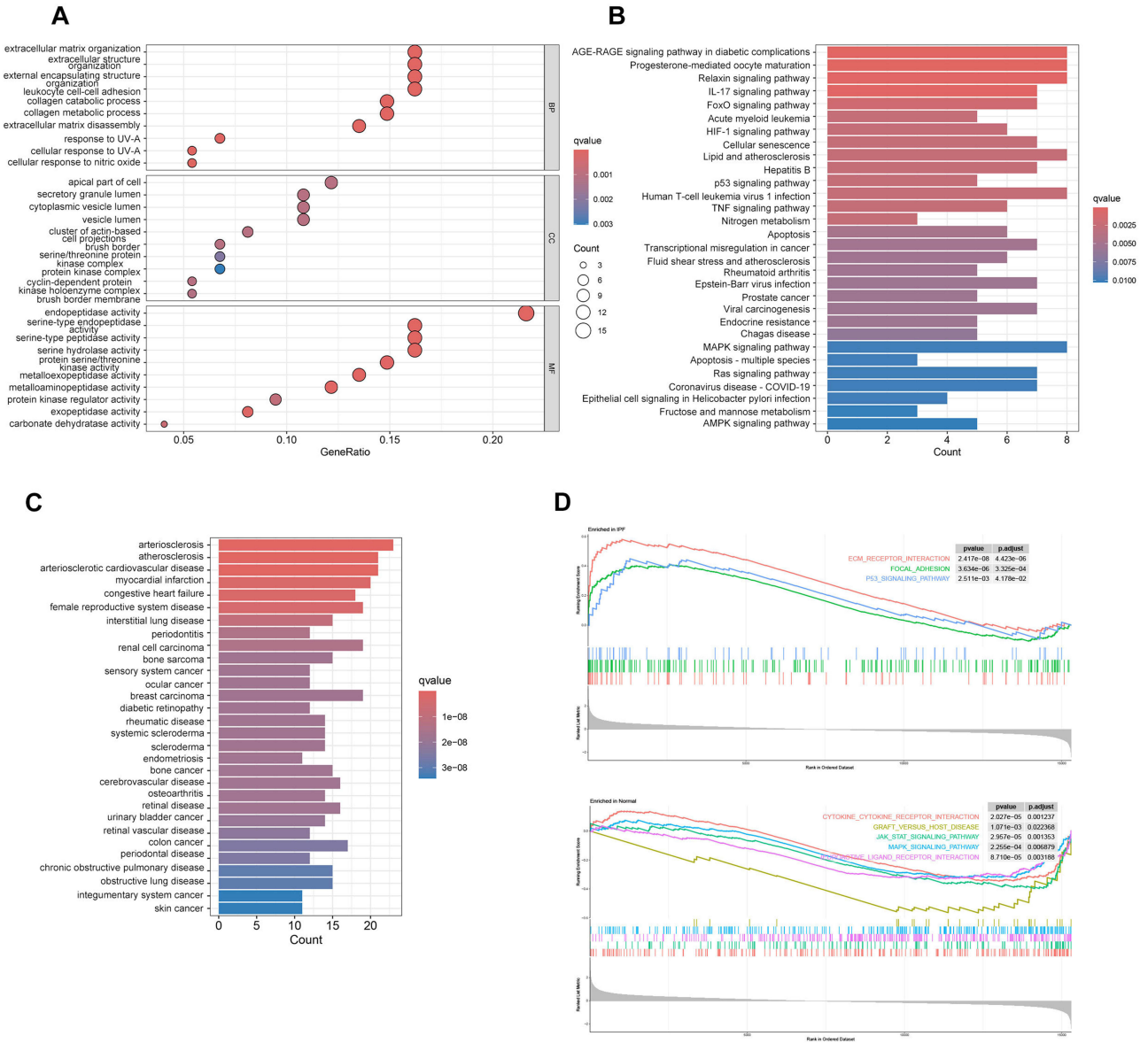

Figure 3 Functional Analysis of Common Targets of SAL in IPF Treatment: (**A**) GO analysis of the intersection of IPF DEGs and SAL target genes. (**B**) KEGG pathway enrichment analysis of the intersection of IPF DEGs and SAL target genes. (**C**) DO analysis of the intersection of IPF DEGs and SAL target genes. (**D**) GSEA results show the top 3 KEGG pathways enriched in the IPF group and the top 5 KEGG pathways enriched in the normal group. $P_{FDR} < 0.05$.

in the normal group, and significant upregulation of ECM-receptor interaction, focal adhesion, and P53 signaling pathways in the IPF group (Figure 3D).

Machine Learning and Molecular Screening of Core Targets of SAL in IPF Treatment

To further enhance the reliability of target prediction, LASSO logistic regression and SVM-RFE were applied to identify the core targets of SAL in combating IPF. The LASSO algorithm identified 18 characteristic genes (Figure 4A), while the SVM-RFE algorithm screened 22 characteristic genes (Figure 4B). Only the overlapping genes, MMP7, ESR2, IGF1, DAO, AKR1B10, VEGFA, TGFBR1, MMP13, and MMP16, were ultimately selected as potential targets for SAL in treating IPF (Figure 4C). We also introduced external datasets for validation, using box plots to verify the expression levels of the target genes and ROC curves to confirm the reliability of the results. In the validation set, we found that eight targets, MMP7, ESR2, IGF1, DAO, AKR1B10, VEGFA, MMP13, and MMP16, demonstrated good specificity ($P_{FDR}<0.05$) (Figure 4D and E). To validate the interaction affinity between SAL and the potential targets, eight significantly different targets were selected for molecular docking and visualization for subsequent experimental validation. The docking results are shown in Supplementary Table 3 and Figure 4F.

Effects of SAL on IGF1, HIF-1α, and MAPK Signaling Pathways

Based on molecular docking results and literature review, we predicted that IGF1 might be a key target of SAL in IPF treatment. Activation of the IGF1 signaling pathway is a crucial mechanism leading to cellular senescence, and insufficient regeneration of alveolar epithelial cells has been confirmed as an important factor in IPF development. Previous studies have shown that inhibiting the IGF1 signaling pathway can effectively improve IPF progression.[27,28] Our study found that exogenous supplementation of SAL significantly reduced IGF1 protein levels in A549 cells compared to the BLM model group (Figure 5A). Cell cycle arrest is a major feature of cellular senescence, and we found that SAL ameliorated BLM-induced S-phase arrest in A549 cells (Figure 5B). Subsequent SA-β-gal staining and counting of A549 cells, along with Western blot analysis of senescence markers p16 and p21 (Figure 5A–C), indicated that increasing concentrations of SAL significantly improved senescence in A549 cells.

KEGG analysis revealed that potential targets of SAL in IPF treatment are closely related to the HIF-1α signaling pathway. Previous studies have confirmed that the HIF-1α/Endoplasmic Reticulum Stress (ERS) signaling pathway is involved in IPF pathogenesis.[29] Western blot analysis showed that SAL treatment significantly reduced the levels of HIF-1α and ERS markers p-IRE1α and ATF6 (Figure 5D and E). Given that HIF-1α induces oxidative stress and mitochondrial damage,[30] we found that SAL treatment significantly improved ROS levels and the degree of mitochondrial damage (Figure 5F and G).

The MAPK signaling pathway plays a crucial role in apoptosis and inflammatory response,[31] and SAL target genes were significantly enriched in KEGG and GSEA analyses. Western blot results showed that BLM treatment activated the MAPK signaling pathway in A549 cells, evidenced by increased p-p38 and p-ERK1/2 ratios compared to p38 and ERK1/2, while SAL treatment effectively reduced this trend (Figure 5H and I). Additionally, the expression levels of inflammation-related markers IL-1β, IL-6, and TNF-α were significantly reduced with increasing concentrations of SAL (Figure 5J).

The experiments demonstrated that SAL significantly reduces IGF1 expression and ameliorates alveolar epithelial cell senescence. Furthermore, SAL improves oxidative stress in alveolar epithelial cells and inhibits inflammatory response and cytokine release via the HIF-1α/ERS and MAPK pathways. Therefore, the anti-IPF mechanism of SAL might be achieved by blocking the IGF1, HIF-1α, and MAPK pathways.

Discussion

In this study, we demonstrated that SAL could alleviate BLM-induced EMT processes in alveolar epithelial cells and the progression of pulmonary fibrosis in mice. Specifically, mice treated with SAL showed significant improvement in alveolar structure damage and inflammatory infiltration, along with reduced fibrous tissue formation. Additionally, SAL reduced EMT marker levels in A549 cells and mouse lungs. Building on this, we used network pharmacology, potential target function analysis, machine learning, and molecular docking to further screen potential targets and pathways of SAL, exploring its anti-IPF molecular mechanisms. It is noteworthy that several other natural compounds have been previously explored for their anti-

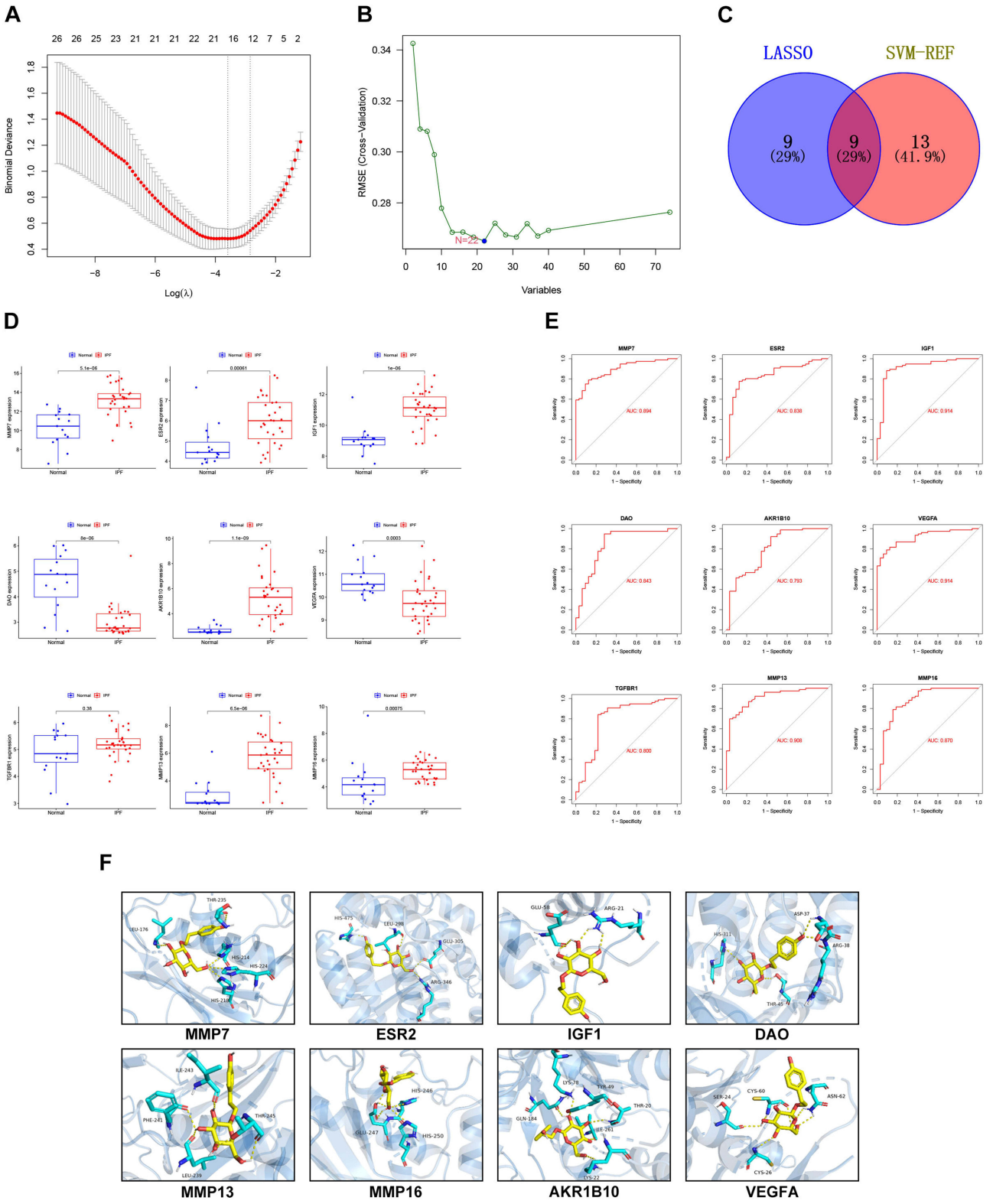

Figure 4 Machine Learning and Molecular Screening of Core Targets of SAL in IPF Treatment: (**A**) Selection of characteristic genes using the LASSO algorithm. (**B**) Selection of characteristic genes using the SVM-RFE algorithm. (**C**) Venn diagram showing the intersection of LASSO algorithm and SVM-RFE algorithm. (**D**) Box plots showing the expression of target genes (MMP7, ESR2, IGF1, DAO, AKR1B10, VEGFA, TGFBR1, MMP13 and MMP16) between normal and IPF samples in the training set. (**E**) ROC analysis of target genes in test sets. (**F**) Molecular docking results of SAL with eight key targets. $P_{FDR} < 0.05$.

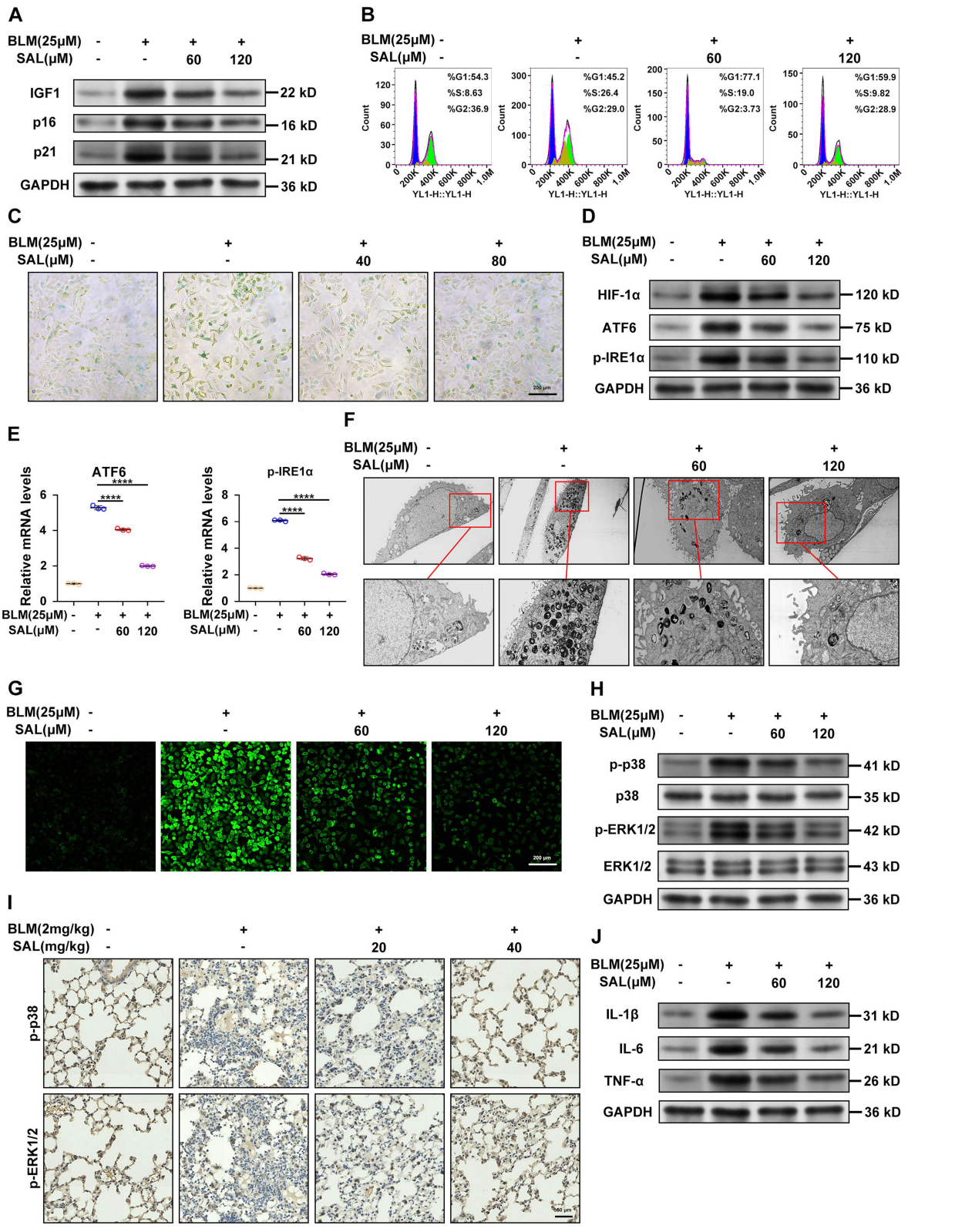

Figure 5 Effects of SAL on IGF1, HIF-1α, and MAPK Signaling Pathways: (**A**) Western blot analysis of IGF1, p16, and p21 protein levels in A549 cells after SAL treatment. (**B**) Cell cycle analysis of A549 cells after treatment with BLM and different concentrations of SAL. (**C**) SA-β-gal staining in A549 cells. (**D**) Western blot analysis of HIF-1α, ATF6, and p-IRE1αprotein levels in A549 cells after SAL treatment. (**E**) The mRNA levels of endo-plasmic reticulum stress markers ATF6 and p-IRE1α in A549 cells after SAL treatment were measured by qRT-PCR. (**F**) Electron microscopy images of A549 cells after SAL treatment. (**G**) ROS levels in A549 cells after SAL treatment. (**H**) Western blot analysis of p-p38, p38, p-ERK1/2, and ERK1/2 protein levels in A549 cells after SAL treatment. (**I**) Representative IHC images of p38 and p-ERK1/2. (**J**) Western blot analysis of inflammatory cytokines IL-1β, IL-6, and TNF-α protein levels in A549 cells after SAL treatment. Scale bars represent 100 μm in (**C** and **G**), 50 μm in (**I**). In (**A–J**), - represents no drug treatment, and + represents drug treatment. Data in (**B** and **E**) are presented as mean ± SD (n = 3, ****P < 0.0001; Student's *t*-test).

fibrotic and anti-inflammatory properties in fibrotic diseases. Curcumin is known for its anti-inflammatory and antioxidant properties, showing promise in preventing fibrosis in preclinical studies.[32] It targets the TGF-β pathways, similar to SAL, but its poor bioavailability limits its therapeutic efficacy.[33] Epigallocatechin gallate (EGCG), found in green tea, has been studied for its ability to modulate the TGF-β/Smad signaling pathway, a crucial mechanism in fibrosis progression.[34] However, its clinical application in IPF remains unconfirmed. Resveratrol, another compound with anti-inflammatory and anti-fibrotic properties, inhibits TGF-β signaling, reduces oxidative stress, and shows potential in preventing pulmonary fibrosis.[35] Nevertheless, side effects such as cytotoxic effects, DNA breaks, and Interaction with other drugs limit its broader use.[36] While curcumin, EGCG, and resveratrol have demonstrated potential anti-fibrotic effects, SAL stands out due to its multi-target approach, modulating various signaling pathways such as IGF1, HIF-1α, and MAPK, offering a more comprehensive mechanism for the treatment of IPF and other fibrotic diseases. Moreover, SAL has shown promising effects in various models of inflammation and organ fibrosis, including myocardial fibrosis,[37] renal fibrosis[22] and liver fibrosis,[38] suggesting its potential broad application in treating pulmonary fibrosis.

Based on LASSO logistic regression and SVM results, we identified nine potential targets, among which MMP7, ESR2, IGF1, DAO, AKR1B10, VEGFA, MMP13 and MMP16 showed significant differences. During molecular docking, these eight target proteins exhibited high binding affinity with SAL. Combining analysis results and literature review, we propose that the anti-fibrotic mechanism of SAL might involve inhibiting the IGF1 signaling pathway. Studies have found that the IGF1 pathway is a key regulator of cell metabolism and senescence, inhibiting its transmission can extend mouse lifespan and improve heart aging.[39] Current research has already explored targeting the IGF1 signaling pathway as a treatment for IPF.[40] In this study, we first found that SAL reduced IGF1 expression levels and improved various senescence phenotypes. Additionally, we discovered significant enrichment of the HIF-1α signaling pathway in KEGG analysis. Previous studies have demonstrated that HIF-1α and the ERS signaling pathway play crucial roles in the pathogenesis of pulmonary fibrosis.[23] HIF-1α can be activated under hypoxic conditions and induces ERS, leading to apoptosis of alveolar epithelial cells. Furthermore, HIF-1 has been shown to upregulate the expression of various pro-inflammatory cytokines, which can trigger the production of ROS through multiple pathways, exacerbating oxidative stress.[41] For instance, increased levels of pro-inflammatory cytokines such as IL-1β and TNF-α may enhance oxidative stress.[42] Although HIF-1 typically activates certain antioxidant genes to protect cells, it may also inhibit antioxidant defense mechanisms under certain pathological conditions. The excessive activation of HIF-1 could interfere with the function of the Nrf2 pathway, a critical regulator of cellular antioxidant defenses, potentially reducing the cell's ability to clear ROS and thereby intensifying oxidative stress.[43] In this study, we found that SAL treatment effectively reduces the expression levels of HIF-1α in alveolar epithelial cells, alleviates ERS, and decreases intracellular ROS levels, thereby protecting the function of the endoplasmic reticulum and mitochondria. MAPKs are important members of the serine/threonine protein kinase family and play key roles in the pathophysiology of various diseases, including inflammation, fibrosis, and cancer.[44] Numerous studies have shown that the MAPK signaling pathway is significantly involved in fibrosis of major organs such as the myocardium, kidneys, and lungs.[45–47] The activation of the MAPK signaling pathway mediates EMT in the process of pulmonary fibrosis, leading to an increase in extracellular matrix secretion by fibroblasts. Zhu et al demonstrated that targeted inhibition of MAPK could significantly improve lung inflammation in mice.[48] In our study, SAL was shown to inhibit the phosphorylation of p38 and ERK1/2, thereby preventing the activation of the MAPK signaling pathway and exerting anti-pulmonary fibrosis effects.

In conclusion, SAL exerts its protective effects against AECs EMT and fibrotic collagen deposition by inhibiting the IGF1, HIF-1α, and MAPK signaling pathways. These actions are attributed to SAL's anti-aging, antioxidant, and anti-inflammatory properties. As a natural compound derived from TCM, SAL shows potential as a therapeutic agent for IPF. In future studies, we will explore the safety evaluation of SAL in animal experiments by incorporating approaches such as network toxicology. We will utilize metabolomics to comprehensively understand the changes in metabolites following SAL intervention. Based on this, we aim to develop effective administration methods to enhance bioavailability and provide an experimental foundation for the translational application of SAL.

Conclusion

In conclusion, our study provides evidence that SAL effectively ameliorates IPF through a multifaceted approach that targets key pathways, including IGF1, HIF-1α, and MAPK. The innovative application of machine learning, network pharmacology, and molecular docking in identifying critical target genes and pathways underscores the novelty of our findings and positions SAL as a promising multi-target therapeutic candidate for IPF. While further research is essential to elucidate the comprehensive mechanisms and safety profile of SAL in IPF treatment, these results highlight its potential as a therapeutic strategy for treating this challenging disease.

Data Sharing Statement

Existing datasets are available in a publicly accessible repository: Publicly available datasets were analyzed in this study. This data can be found here: GEO database (www.ncbi.nlm.nih.gov/geo/): GSE21369, GSE10667, GSE110147 and GSE24206.

Funding

This research was funded by National Natural Science Foundation of China, grant number 81870388.

Disclosure

All authors declare that there are no conflicts of interest.

References

1. Ling Y, Qu L, Jianjun D et al. Ginsenoside Rh4 alleviates idiopathic pulmonary fibrosis by enhancing the CXCL9–CXCR3 axis. *Food Front*. 2024;5:0325. doi:10.1002/fft2.388
2. Basavaraj V, Chanabasayya V. Study on potential differentially expressed genes in idiopathic pulmonary fibrosis by bioinformatics and next generation sequencing data analysis. *bioRxiv*. 2023;20:1. doi:10.1101/2023.09.18.558229
3. Anna JP, Carey CT, Martine RJ, et al. Idiopathic pulmonary fibrosis: state of the art for 2023. *Europ resp J*. 2023;61:126. doi:10.1183/13993003.009572022
4. Barbara R, Riccardo P, Paola C, et al. Gastroesophageal reflux disease in idiopathic pulmonary fibrosis: viewer or Actor? To treat or not to treat? *Pharmaceuticals*. 2022;15:0822. doi:10.3390/ph15081033
5. Saha P, Talwar P. Idiopathic pulmonary fibrosis (IPF): disease pathophysiology, targets, and potential therapeutic interventions. *Mol Cell Biochem*. 2023;479:0914. doi:10.1007/s11010-023-04845-6
6. Francesco B, Paolo S, Ryerson CJ. Current and future treatment landscape for idiopathic pulmonary fibrosis. *Drugs*. 2023;83:1026. doi:10.1007/s40265-023-01950-0
7. Banu AK-S, Badrul AC. Forced vital capacity in idiopathic pulmonary fibrosis — FDA review of pirfenidone and nintedanib. *New Engl J Med*. 2015;372:0326. doi:10.1056/nejmp1500526
8. Sykes D, Day E, Ibrar K, et al. Adverse effects of nintedanib – a portent of gender inequality? *Eur Respiratory Soc*. 2023;2023:0909. doi:10.1183/13993003.congress-2023.pa2876
9. Jürgen B, Steven DN, Wim W, et al. Efficacy and safety of sildenafil added to pirfenidone in patients with advanced idiopathic pulmonary fibrosis and risk of pulmonary hypertension: a double-blind, randomised, placebo-controlled, Phase 2b trial. *Lancet Respir Med*. 2021;9:0101. doi:10.1016/s2213-2600(20)30356-8
10. Paolo S. Pirfenidone and mortality in idiopathic pulmonary fibrosis. *Lancet Respir Med*. 2017;5:0101. doi:10.1016/s2213-2600(16)30416-7
11. Hao S, Nu Z, Yuqing L, et al. The interaction between pulmonary fibrosis and COVID-19 and the application of related anti-fibrotic drugs. *Front Pharmacol*. 2022;12:805535. doi:10.3389/fphar.2021.805535
12. Κατερίνα A, Konstantinos K, Nikos T. Mesenchymal stem cell treatment for IPF—time for phase 2 trials? *Lancet Respir Med*. 2017;5:0601. doi:10.1016/s2213-2600(17)30180-7
13. Adam G. Lung transplantation disparities among patients with IPF: recognition and remedy. *Ann Am Thorac Soc*. 2022;19:0601. doi:10.1513/annalsats.202202-123e
14. Meihua J, Chun W, Yu X, et al. Pharmacological effects of salidroside on central nervous system diseases. *Biomed Pharmacother*. 2022;156:1201. doi:10.1016/j.biopha.2022.113746
15. Christopher GB, Shelby BM, Abby CW, Mallory RM, John KP, Rebecca RR. Effects of acute golden root extract (rhodiola Rosea) supplementation on anaerobic exercise capacity. *Med Sci Sports Exerc*. 2018;50:721. doi:10.1249/01.mss.0000538375.55554.ab
16. Hua-En L, Enoch T, Jude C, Cheng Chang H. 25891 the effects of Chinese herbal medicine rhodiola rosea on preventing photoaging in keratinocytes. *J Am Acad Dermatol*. 2021;85:AB74. doi:10.1016/j.jaad.2021.06.320
17. Tyler DW, Haley L, Caleb CR, Rebecca RR, Christopher GB. Effects of short-term golden root extract (Rhodiola rosea) supplementation on resistance exercise performance. *Int J Environ Res Public Health*. 2021;18:0629. doi:10.3390/ijerph18136953
18. Michael PT-S, Tomáš P, Fu-Shuang L, Valentina C, Jing-Ke W. Complete pathway elucidation and heterologous reconstitution of rhodiola salidroside biosynthesis. *Mol Plant*. 2018;11:205. doi:10.1016/j.molp.2017.12.007
19. Yanlei X, Yueming W, Yanlei X, Wei G, Li T. Salidroside alleviated hypoxia-induced liver injury by inhibiting endoplasmic reticulum stress-mediated apoptosis via IRE1α/JNK pathway. *Biochem Biophys Res Commun*. 2020;529:0801. doi:10.1016/j.bbrc.2020.06.036

20. Xue L, Chunzhi C, Jingzhi J, et al. Salidroside mitigates airway inflammation in asthmatic mice via the AMPK/Akt/GSK3β signaling pathway. *Int Arch Allergy Immunol*. 2021;183:1011. doi:10.1159/000519295
21. Kuo-Cheng L, Seh-Huang C, Hsiao-Yi W, et al. Salidroside ameliorates sepsis-induced acute lung injury and mortality via downregulating NF-κB and HMGB1 pathways through the upregulation of SIRT1. *Sci Rep*. 2017;7:0920. doi:10.1038/s41598-017-12285-8
22. Rui L, Yi G, Yiming Z, Xue Z, Lingpeng Z, Tianhua Y. Salidroside ameliorates renal interstitial fibrosis by inhibiting the TLR4/NF-κB and MAPK signaling pathways. *Int J Mol Sci*. 2019;20:0304. doi:10.3390/ijms20051103
23. Xue L, Shiyao C, Wenle L, Hongqing X, Liangen S. Elucidation of the anti-colon cancer mechanism of Phellinus baumii polyphenol by an integrative approach of network pharmacology and experimental verification. *Int J Biol Macromol*. 2023;253:1201. doi:10.1016/j.ijbiomac.2023.127429
24. Ji-Hoon C, Richard G, Kai W, et al. Systems biology of interstitial lung diseases: integration of mRNA and microRNA expression changes. *BMC Med Genomics*. 2011;4:0117. doi:10.1186/1755-8794-4-8
25. Kazuhiko K, Kevin FG, Kathleen OL, et al. Gene expression profiles of acute exacerbations of idiopathic pulmonary fibrosis. *Am J Respir Crit Care Med*. 2009;180:0715. doi:10.1164/rccm.200810-1596oc
26. Matthew JC, Karishma H, Christopher JH, Mariamma J, Marco M. Comprehensive gene expression profiling identifies distinct and overlapping transcriptional profiles in non-specific interstitial pneumonia and idiopathic pulmonary fibrosis. *Respir Res*. 2018;19:0815. doi:10.1186/s12931-018-0857-1
27. Wei S, Xiaoyan J, Xiaoyu Y, et al. Regulation of the IGF1 signaling pathway is involved in idiopathic pulmonary fibrosis induced by alveolar epithelial cell senescence and core fucosylation. *Aging*. 2021;13:0730. doi:10.18632/aging.203335
28. Huijuan X, Xiaoxi H, Shiyao W, et al. 1143:Metformin ameliorates bleomycin-induced pulmonary fibrosis in mice by suppressing IGF-1. *Crit Care Med*. 2020:0101. doi:10.1097/01.ccm.0000643508.83802.5f
29. Shanchen W, Fei Q, Yanping W, Xinmin L. Overexpression of KLF4 suppresses pulmonary fibrosis through the HIF-1α/endoplasmic reticulum stress signaling pathway. *Int J Mol Sci*. 2023;24:0912. doi:10.3390/ijms241814008
30. Hong D, Cheng-Yi T, Wei W, Ying P, Rui-Qing J, Ling-Dong K. Polydatin ameliorates high fructose-induced podocyte oxidative stress via suppressing HIF-1α/NOX4 pathway. *Pharmaceutics*. 2022;14:1016. doi:10.3390/pharmaceutics14102202
31. De Maeyer RP, van de Merwe RC, Louie R Blocking elevated p38 MAPK restores efferocytosis and inflammatory resolution in the elderly. *Nat Immunol*. 2020;21:615. doi:10.1038/s41590-020-0646-0
32. Namitosh T, Digvijay S, Debabrata D, Rashmi S. Curcumin modulates paraquat-induced epithelial to mesenchymal transition by regulating Transforming Growth Factor-β (TGF-β) in A549 cells. *Inflammation*. 2019;42:0426. doi:10.1007/s10753-019-01006-0
33. Cihui T, Sajid A, Yifan W, et al. Improving intestinal absorption and oral bioavailability of curcumin via taurocholic acid-modified nanostructured lipid carriers. *Int j Nanomed*. 2017;2017:1001. doi:10.2147/ijn.s145988
34. Rattiyaporn K, Paleerath P, Angkhana N, Sirikanya P, Kanyarat S, Visith T. Epigallocatechin-3-gallate prevents TGF-β1-induced epithelial-mesenchymal transition and fibrotic changes of renal cells via GSK-3β/β-catenin/Snail1 and Nrf2 pathways. *J Nutr Biochem*. 2020;76:0201. doi:10.1016/j.jnutbio.2019.108266
35. Sara Hassan Hassan A, Mahmoud AM, Rania AHI, Nahed DM. Customizable resveratrol spray-dried micro-composites for inhalation as a promising contender for treatment of idiopathic pulmonary fibrosis. *Int J Pharm*. 2023;642:0701. doi:10.1016/j.ijpharm.2023.123117
36. Abdullah S, Anna Maria P, Nadin Y, et al. Potential adverse effects of resveratrol: a literature review. *Int J Mol Sci*. 2020;21:0318. doi:10.3390/ijms21062084
37. Jie M, Yujie L, Jun X, Anqi W, Yue L, Lihong M. Integrating network pharmacology and experimental verification to explore the mechanisms of salidroside against myocardial fibrosis. *Biochem Biophys Res Commun*. 2023;677:1001. doi:10.1016/j.bbrc.2023.07.059
38. Qiannan Y, Yang Z, Changqing Z, Li X, Ping J. Salidroside inhibits CCl4-induced liver fibrosis in mice by reducing activation and migration of HSC induced by liver sinusoidal endothelial cell-derived exosomal SphK1. *Front Pharmacol*. 2021;12:0513. doi:10.3389/fphar.2021.677810
39. Mahmoud A, Viktoria T-H, Alexander Martin H, et al. Fine-tuning cardiac insulin-like growth factor 1 receptor signaling to promote health and longevity. *Circulation*. 2022;145:0621. doi:10.1161/circulationaha.122.059863
40. Danielle MH, Jeong Han K, Malay C, et al. IPF pathogenesis is dependent upon TGFβ induction of IGF-1. *FASEB J*. 2020;34:0217. doi:10.1096/fj.201901719
41. Dan W, Lihong W, Yu Z, Yapeng L, Li Z. Hypoxia regulates the ferrous iron uptake and reactive oxygen species level via divalent metal transporter 1 (DMT1) Exon1B by hypoxia-inducible factor-1. *IUBMB Life*. 2010;62:0728. doi:10.1002/iub.363
42. Kuan Chou C, Changrong C, Chang Yu C, Kai-Yi T, Chiung Chi P, Robert YP. Bicalutamide elicits renal damage by causing mitochondrial dysfunction via ROS damage and upregulation of HIF-1. *Int J Mol Sci*. 2020;21:0511. doi:10.3390/ijms21093400
43. Andrea BZ, Adalberto P, Rodrigo C, Carolina AF, Víctor MP, Jorge GF. Cellular and molecular mechanisms in the hypoxic tissue: role of HIF-1 and ROS. *Cell Biochem Funct*. 2013;31:0613. doi:10.1002/cbf.2985
44. Xiaomei Q, Guan C. p38γ MAPK inflammatory and metabolic signaling in physiology and disease. *Cells*. 2023;12:0621. doi:10.3390/cells12131674
45. Juan H, Xi W, Sijie W, Yuqi T, Qin Z, Congxin H. Activin A stimulates the proliferation and differentiation of cardiac fibroblasts via the ERK1/2 and p38-MAPK pathways. *Eur J Pharmacol*. 2016;789:1001. doi:10.1016/j.ejphar.2016.07.053
46. Zhenzhen L, Xianghua L, Baoying W, et al. Pirfenidone suppresses MAPK signalling pathway to reverse epithelial-mesenchymal transition and renal fibrosis. *Nephrology*. 2017;22:0706. doi:10.1111/nep.12831
47. Naonori SS, Michiaki K, Tetsuji Y. Inhibition of the p38 MAPK pathway ameliorates renal fibrosis in an NPHP2 mouse model. *Nephrol Dial Transplant*. 2011;27:1109. doi:10.1093/ndt/gfr550
48. Wenxiang Z, Qi D, Lu W, et al. Vitamin D3 alleviates pulmonary fibrosis by regulating the MAPK pathway via targeting PSAT1 expression in vivo and in vitro. *Int Immunopharmacol*. 2021;101:1201. doi:10.1016/j.intimp.2021.108212